

Towards Sustainable Computing: Assessing the Carbon Footprint of Heterogeneous Systems

Vidya A. Chhabria¹, Chetan Choppali Sudarshan¹, Sarma Vrudhula¹, and Sachin S. Sapatnekar²
¹Arizona State University; ²University of Minnesota

Abstract—Decades of progress in energy-efficient and low-power design have successfully reduced the operational carbon footprint in the semiconductor industry. However, this has led to an increase in embodied emissions, encompassing carbon emissions arising from design, manufacturing, packaging, and other infrastructural activities. While existing research has developed tools to analyze embodied carbon at the computer architecture level for traditional monolithic systems, these tools do not apply to near-mainstream heterogeneous integration (HI) technologies. HI systems offer significant potential for sustainable computing by minimizing carbon emissions through two key strategies: “reducing” computation by reusing pre-designed chiplet IP blocks and adopting hierarchical approaches to system design. The reuse of chiplets across multiple designs, even spanning multiple generations of integrated circuits (ICs), can substantially reduce embodied carbon emissions throughout the operational lifespan. This paper introduces a carbon analysis tool specifically designed to assess the potential of HI systems in facilitating greener VLSI system design and manufacturing approaches. The tool takes into account scaling, chiplet and packaging yields, design complexity, and even carbon overheads associated with advanced packaging techniques employed in heterogeneous systems. Experimental results demonstrate that HI can achieve a reduction of embodied carbon emissions up to 70% compared to traditional large monolithic systems. These findings suggest that HI can pave the way for sustainable computing practices, contributing to a more environmentally conscious semiconductor industry.

I. INTRODUCTION

All aspects of computing, from small chips to large datacenters, come with a carbon footprint (CFP) price tag. For several decades, the semiconductor industry has focused on making chips smaller, faster, and less power-hungry, but few efforts have considered the impact on the environment. The dramatic increase in the demand for compute in the past two decades, fueled by new applications (e.g., artificial intelligence) that demand at-edge and at-cloud-scale computing, has resulted in the information and computing technology (ICT) sector contributing to more than 2% of the world’s CFP [1] – half that of the aviation industry [2] and projected to surpass it in the next decade if left unchecked.

Fig. 1 shows the life cycle assessment (LCA) of an electronic product and highlights the different sources of greenhouse gases (GHG) in the life of a semiconductor component. The operational costs are the end-user-generated CFP which in the case of a data center are the data-to-day activities that draw energy, while the embodied costs are the costs that come from design, manufacturing, packaging, and materials sourcing of the server class compute resources in the datacenter.

While technology scaling and electronic design automation

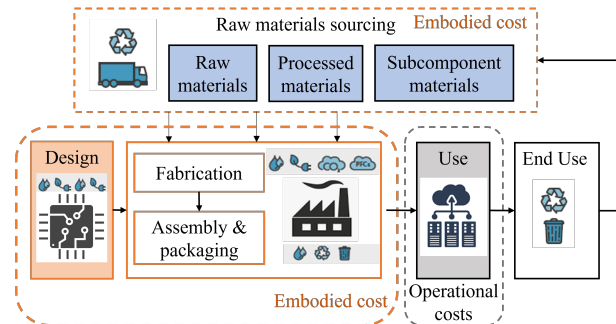


Fig. 1. Embodied and operational CFP in the semiconductor supply chain [3].

(EDA) have helped design energy-efficient VLSI systems with lower operational CFP, the environmental footprint has still been increasing over the past decade and is dominated by carbon emissions from chip design and manufacturing [3]–[5]. It is imperative to look beyond low power and energy-efficiency-driven metrics for VLSI system design, and it is essential to use embodied carbon emissions as a direct optimization metric. For sustainable use of today’s modern computing, there is a need for design techniques that not only meet the power, performance, and area (PPA) targets of today’s systems but also consider the CFP. Several technology companies have pledged to limit their CFP [6]–[8], and this can only be achieved by adopting approaches that are cognizant of the embodied CFP.

Two prior bodies of work focus on embodied CFP estimation at the architectural level: the first [9], [10] and the second [4], [11]. The work in [10] reformulated the Kaya identity [12] to understand how the global CFP of computer systems evolves over time and has made a case to lower chip sizes to lower embodied CFP and [9] creates a very simple model based on first principles. The work in [4], [11] has created a data-driven model, from publicly available sustainability reports from industry [3], [6], [7], [13], for embodied carbon estimation for a given input hardware architecture and has created a platform for carbon-aware design space exploration (DSE). While these works have set a new paradigm toward sustainable computing, they are limited in scope:

- 1) They do not accurately consider the overheads for packaging, which is crucial for heterogeneous systems. ACT [4] uses a fixed value that does not consider the size of the package, the yield of the package, or the assembly process, while [10] does not consider any CFP from packaging.
- 2) They do not apply to heterogeneous systems with chiplets

in different technology nodes integrated into a single advanced package which is near-mainstream today.

- 3) They do not consider the carbon that comes from the design of individual chips/chiplets, which, even though amortized across all manufacturing components, is a significant contributor to the total embodied CFP.

Also, prior package-level carbon analysis tools have been limited to only ball grid arrays and monolithic flip-chip technologies [14] and have not been studied in the context of sustainable computing or HI.

With Moore’s law slowing down and SRAM and analog components not scaling [15], [16], the way forward towards sustaining Moore’s law to the era of trillion-transistor systems and beyond is through HI [17], [18]. Instead of building system functionality on a single die, HI integrates a set of chiplets, each corresponding to the single die of today, onto a substrate that enables high-density, high-bandwidth chiplet-to-chiplet interconnections. Recent and upcoming advances in HI, including the rapid shrinking of bond pitches between chiplets and interposers [19]–[23], are enabling the design of increasingly sophisticated integrated systems. This calls for carbon modeling tools at the architecture level that can model HI systems and not just monolithic dies as in [4]. New CFP models must be created that account for packaging overheads, silicon fabrics, and multi-die system integration in different technology nodes. These modeling tools can be embedded into still-evolving HI design methodologies to optimize HI systems for power, performance, area, and carbon (PPAC).

Inspired by the principles of environmental sustainability – the three R’s of “reduce, reuse, and recycle” – in this paper, we evaluate the potential of HI systems towards sustainable computing by developing a carbon analysis tool to measure design, manufacturing, and packaging CFP for heterogeneous systems. HI systems have a potential for sustainable computing by “reducing” carbon emissions by reducing the computation involved in designing each component from scratch and by “reusing” pre-designed chiplet IP blocks through hierarchical approaches. The ability to reuse chiplets across several designs not only in the current generation of ICs but even in the next generation can massively amortize the embodied CFP.

In this paper, we introduce an embodied CPF estimator specifically tailored for heterogeneous systems that incorporate advanced packaging architectures. Our goal is to demonstrate the potential of such systems in reducing CFP compared to large monolithic dies, even when accounting for the overhead associated with advanced packaging techniques. To estimate the manufacturing CFP of chiplets in heterogeneous systems, we extend existing models from [4] and [5] with modifications to account for area, yield, defect densities, and energy-efficiency of process equipment which all scale as the technology matures. Our packaging CFP models account for four types of wafer-level packaging architectures: RDL Fan-out, silicon bridges such as embedded multi-die interconnect bridge (EMIB), passive interposers, and active interposers. Further, we also consider the overheads with respect to inter-die whitespace and additional inter-die routing overheads as

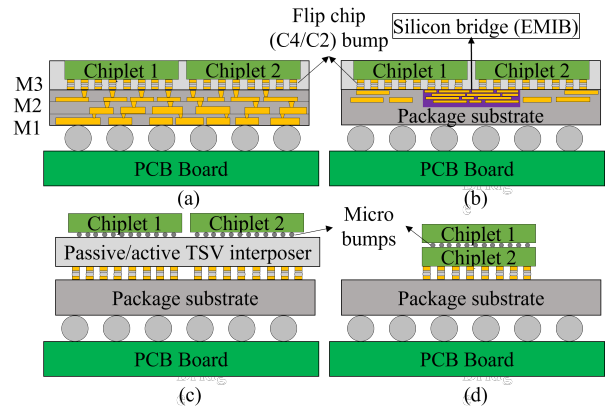


Fig. 2. Packaging architectures: (a) RDL fanout packaging in EMC, (b) thin-film and silicon bridge architecture (Intel’s EMIB, TSMC’s LSI), (c) 2.5D integration with active or passive interposers and (4) 3D integration.

a part of the packaging CFP estimation. For design CFP, we employ a simplified model based on design compute time and EDA tool productivity with every technology node, to predict the carbon emissions associated with the design phase.

The key contributions of our paper are as follows:

- 1) To the best of our knowledge, this is the first work to propose HI as a direction toward sustainable computing.
- 2) We develop a carbon analysis tool to estimate the embodied CFP (design, manufacturing, and packaging) of HI systems, accounting for a variety of packaging architectures, scaling, yield, process equipment energy efficiency, and EDA tool productivity.
- 3) We build a novel HI packaging CFP estimator to predict the advanced packaging overhead costs, considering whitespaces on the package substrate and inter-die communication overheads.
- 4) We evaluate our tool and the potential HI has in reducing embodied CFP on a diverse set of industry testcases (mobile processors, GPUs, and CPUs) and find that HI systems can reduce embodied CFP by upto 70%.

II. HI AND ITS SCOPE FOR SUSTAINABLE COMPUTING

A. HI and different packaging architectures

HI has offered a feasible approach for cost-effective chip design which can help sustain Moore’s law. An HI system splits a large SoC into multiple smaller dies, referred to as chiplets, where each chiplet may have a different functionality, potentially built in different process nodes or designed by separate vendors reducing both design time and cost. All chiplets are integrated into a single package. An HI system may come in different packaging architectures, as shown in Fig. 2 that vary in cost and complexity. Multi-die heterogeneous systems can have anywhere between two chiplets to tens of different chiplets and depending on the number of chiplets, budgeted cost, and complexity, the choice of packaging architecture for heterogeneous systems is different [24]. We describe four commonly used advanced packaging and integration technologies: (1) *RDL fan-out integration* As shown in Fig. 2(a), it involves the integration of multiple chiplets on a package substrate or fan-out redistribution layer (RDL) substrate. Typically the

package substrate consists of 3-4 RDL metal layers with linewidths and spacings (L/S) varying from 6/6 to 10/10 μm .

(2) *Thin film and silicon bridge-based integration* In this integration technology, the package substrate has thin-film layers defined as embedding fine metal RDLs or a silicon bridge on top of a build-up organic package substrate or in a fan-out epoxy molding compound (EMC) substrate as highlighted in Fig. 2(b). Intel’s embedded multi-die interconnect bridge (EMIB) and TSMC’s local silicon interconnect (LSI) is an example of this technology. The technology uses local silicon bridges to host ultra-fine L/S structures for die-to-die interconnect communications of about 2 μm .

(3) *Passive and active interposer-based integration* This corresponds to multiple chiplets in the package that are supported by a through-silicon via (TSV)-less or TSV-based active/passive interposer, and then attached to a package substrate, as shown in Fig. 2(c). This technology is typically termed as a 2.5D architecture. The active interposer consists of both FEOL and BEOL layers while the passive interposer consists of BEOL layers and are both typically implemented in an older technology node.

(4) *3D integration* Here, active interposers are used to support the chiplets and then attached to the packaging substrate, or multiple chiplets are stacked over the packaging substrate and connected through microbumps, as shown in Fig. 2(d), or direct bumpless bonding [25].

HI has opened up a completely new design space that was previously unexplored by architectural-level carbon simulators [4], [10]. However, the exploration of this space requires the development of models that can account for the different possible design decisions in the HI system that impact the CFP. For instance, each of the above four described packaging architectures differs in their yields, assembly process, and material used and therefore have different CFPs. EMIB consists of high-density interconnects with fine L/S, typically having lower yields compared to the larger RDL layers in fan-out packaging. Interposer-based integration strategies typically use more materials, and layers, and have a more complex manufacturing process compared to the fan-out RDL and EMIB architectures which results in larger CFP. However, the cost overheads from novel packaging techniques in terms of carbon footprint are small when compared to the large benefit from the chip manufacturing yield improvement and design cost reduction [23]. In this work, we evaluate the embodied CFP for these packaging architectures and evaluate the potential HI systems have towards carbon-emission efficient computing.

B. Scope for sustainable computing through HI

HI systems have great potential to lower the embodied CFP associated with design and manufacturing when compared to their monolithic counterparts due to several reasons:

(1) *Yield and area* As we pack more functionality and logic onto the same monolithic IC, the increase in the area increases the CFP due to an increase in materials needed for manufacturing and a decrease in yield. Fig. 3(a) shows a result for a large industry testcase in a 10nm technology. We sweep

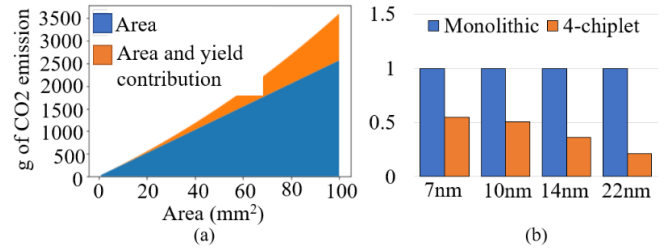


Fig. 3. (a) Embodied CFP in grams (g) of equivalent CO₂ emission versus area. (b) Comparison of manufacturing CFP of the large monolithic NVIDIA GA102 GPU and a 4-chiplet-based architecture of the GPU.

the area of the monolithic SoC and observe an exponential increase in the associated manufacturing CFP due to lower yields. Since a HI system disaggregates the monolithic system into several smaller dies, each die can be manufactured with a significantly lower environmental cost. For example, Fig. 3(b) compares the CFP of a monolithic GA102 testcase against a 4-chiplet representation of the GPU where the memory and analog components are on independent chiplets, and the large digital block is split into two smaller chiplets. The CFP of the 4-chiplet design is normalized to the monolithic design’s CFP for different technology nodes. The 4-chiplet GPU has significantly lower manufacturing CFP even after including the carbon overheads from packaging due to the higher yields of the chiplets when compared to the monolithic chip.

(2) *Technology node* In an HI system, dies can be implemented in different technology nodes. With analog and SRAM blocks not scaling at the same rate as digital logic, several design houses [15], [26] use older technology node chiplets for memory controllers and analog logic. As pointed out in [3], the CFP to manufacture chips in older technology nodes is much lower than for newer technology nodes due to lower defect densities (better yields), fewer lithography steps due to fewer BEOL/FEOL layers, and the better energy-efficiency of lithography equipment involved in manufacturing older technology nodes with today’s latest manufacturing equipment.

(3) *Design time* Reusing existing silicon-proven die not only saves design time directly but also saves the associated design-time CFP. Further, the heterogeneity that allows some chiplets to be built in older nodes is not only easier and lower cost but also comes with lower CFP overheads. Typically, even EDA tools scale with technology, and the latest versions of EDA tools can perform design faster with better quality of results on an older technology node [27] due to continuous improvements made by the EDA industry.

III. EMBODIED CFP ANALYSIS FRAMEWORK

A. Problem statement

In this work, we develop an embodied CFP analysis tool that takes an architectural-level description of a large monolithic SoC or an architectural-level description of the heterogeneous system and a choice of a packaging architecture as input to estimate the total embodied carbon footprint of the system, including chip/chiplet manufacturing CFP, HI packaging CFP, and design CFP as output. We model the total embodied CFP of the system as the sum of the CFP coming from the different

sources highlighted in Fig. 1 and is given by:

$$C_{\text{tot}} = \sum_{i=1}^{N_C} C_{\text{mfg},i} + C_{\text{des}} + C_{\text{HI}} \quad (1)$$

where $C_{\text{mfg},i}$ is the manufacturing CFP of each chiplet, N_C is the number of chiplets, C_{des} is the design CFP of all chiplets, and the HI system, C_{total} is the total embodied CFP, and C_{HI} is contributions from manufacturing and assembly of the advanced package and any inter-die communication overheads.

B. Manufacturing CFP estimation

To estimate the manufacturing CFP of each chiplet, we make three essential modifications to [4] to support the estimation of embodied CFP of a heterogeneous system for system disaggregation as described below:

(1) *Area scaling models*: Since a system disaggregation algorithm or a heterogeneous system requires selecting a technology node for each chiplet, our carbon estimation tool uses transistor density scaling trends from [28], [29] and transistor counts from our testcase architectures to determine the area of a chiplet in a specific technology node. The area scaling models are critical to the estimation of CFP as larger chiplet areas in older technology nodes can have larger CFP even though they have lower CFP per unit area (CFPA). We use three different area scaling models for logic, memory, and analog blocks, as each has different transistor densities and, therefore different areas with every technology node. We evaluate the area of the die as $A_{\text{die}}(d, p) = D_T(d, p) \times N_T$, where $D_T(d, p)$ is the transistor density for design type d and process p , N_T is the number of transistors in the die, and $A_{\text{die}}(d, p)$ is the area of die of type d in process node p .

(2) *Yield models*: One of the primary advantages of HI is the cost savings that come with larger manufacturing yields due to smaller die sizes. The increase in yield compared to a large monolithic die also helps lower CFP. However, if the die is in an older technology node, then $A_{\text{die}}(d, p)$ must be accounted for as an increase in the area may lower yields which also lower CPF, as shown in Fig. 3(a). To estimate the impact of the area on yield and CFP, we use a negative binomial yield distribution model given by [30]–[32]:

$$Y(d, p) = \left(1 + \frac{A_{\text{die}}(d, p) \times D_0(p)}{\alpha} \right)^{-\alpha} \quad (2)$$

where $Y(d, p)$ is the yield of die with area $A_{\text{die}}(d, p)$, $D_0(p)$ is the defect density for process p , α is a clustering parameter. It is important to note that the defect density is also p dependent and scales with technology. On the one hand, legacy nodes have lower defect densities which result in larger yields, and on the other, older technology nodes result in larger A_{die} values leading to lower yields. Our tool considers these tradeoffs while estimating CFP.

(3) *Energy-efficiency of process equipment*: With advances in process equipment, the energy efficiency of every step during photolithography equipment improves, especially on more mature technology nodes. We incorporate the energy efficiency of the equipment as a derate factor (η_{eq}) from [13]. The $C_{\text{mfg},i}$ on a per chiplet basis is given by multiplying the carbon footprint per unit area (CFPA) with the area of the die:

$$C_{\text{mfg},i} = \text{CFPA} \times A_{\text{die}}(d, p) \quad (3)$$

$$\text{CFPA} = \frac{(\eta_{\text{eq}} \times C_{\text{mfg,src}} \times \text{EPA}(p) + C_{\text{gas}} + C_{\text{material}})}{Y(d, p)} \quad (4)$$

where C_{src} is carbon intensity which depends on the energy source of the fab (i.e., renewables vs. non-renewables), which converts the energy consumed into carbon emission. EPA is the energy consumed per unit area during manufacturing of process p and derived from [5], C_{gas} is the CFP from the greenhouse gas emissions, C_{material} is the carbon footprint of sourcing the materials for fabricating the chip/chiplet, and CFPA is the carbon footprint per unit area.

C. HI-oriented CFP overheads

With the projected widespread adoption of HI systems, the cost of packaging is projected to dominate design [33]. Although there are several sustainability reports from large semiconductor manufacturing and design companies, these reports do not specifically break down the contributions from packaging. The prior art in this area has been limited to wire bond packages and flip chip packages [14]. Since HI has opened up a previously unexplored design space, it requires developing models that can account for the different possible design decisions in the HI system that impact the CFP. In particular, decisions related to the choice of the package (architecture) (C_{package}), whitespace on the package substrate or interposer ($C_{\text{whitespace}}$), and inter-die communication ($C_{\text{mfg,comm}}$). In our work, we measure the CFP from these three sources as described below: (1) *Package-related overheads* (C_{package}): We develop models for the four 2.5D packaging architectures, including RDL fan-out, silicon bridge, passive and active interposers based on architectural descriptions, materials, and packaging technology nodes from [24], CFP estimates from [5], and packaging industry reports [34]–[36].

(a) *RDL Fan-out*: This packaging architecture uses an epoxy molding compound (EMC) substrate with RDL metal layers patterned to make connections between the chiplets as shown in Fig. 2(a). Our CFP model uses the energy per unit area per metal layer (EPLA) from a manufacturing fab to determine CFP overheads with the RDL layers. Based on the number of layers, the yield of the layers, and EPLA, we determine the embodied CFP of an RDL package as:

$$C_{\text{RDL}} = \frac{L_{\text{RDL}} \times \text{EPLA}_{\text{RDL}}(p) \times C_{\text{pkg,src}} \times A_{\text{package}}}{Y(\text{RDL}, p)} \quad (5)$$

where $\text{EPLA}_{\text{RDL}}(p)$ is the energy consumed in patterning a single RDL layer in process p per unit area, $C_{\text{pkg,src}}$ is the carbon intensity of the packaging fab which is based on the source of energy (renewable or non-renewable sources), L_{RDL} is the number of layers of RDL in the package substrate, $Y(\text{RDL}, p)$ is the yield of the RDL in process p estimated using Equation (2), and A_{package} . The area of the package substrate is estimated after considering the whitespace and routing overheads and described later in this section.

(b) *Silicon bridge*: A silicon bridge is a high-density intercon-

nect between two chiplets, and we model its CFP similar to the CFP of the RDL fan-out-based package except that they have lower linewidth and spacing (L/S) and, therefore, lower yields when compared to RDL fan-out. The yields are lower due to the lower bond pitches between the chiplets and the bridges and the cavity-based fabrication of the bridge in the package substrate. For our model, we use the EPLA values from [5] for an advanced technology node lower metal layer with ultra-fine L/S. These high-density interconnects do not span the entire area of the package substrate but are local to a region in the package based on the floorplan of the chiplets. The number of silicon bridges and their placement depends on the chiplet flooplan and bandwidth requirements. In our work, we consider a bridge ranges and typical bridge areas from Intel’s EMIB silicon bridge specification [37] as input to determine the number of bridges that must be used. If the two adjacent dies that must be connected through silicon bridges have overlapping die edges larger than the range, then an additional bridge is added. The CFP of a silicon bridge-based packaging architecture is given by:

$$C_{\text{bridge}} = \frac{N_{\text{bridge}} \times L_{\text{bridge}} \times \text{EPLA}_{\text{bridge}}(p) \times C_{\text{pkg, src}} \times A_{\text{bridge}}}{Y(\text{bridge}, p)} \quad (6)$$

where L_{bridge} is the number of metal layers in the bridge, A_{bridge} is the area occupied by the silicon bridge in the package substrate, N_{bridge} is the number of silicon bridges, $Y(\text{bridge}, p)$ is the yield of fabricating the silicon bridge in process p in the bridge cavity, $\text{EPLA}_{\text{bridge}}(p)$ is the energy per unit layer per unit area of patterning the silicon bridge in process p .

(c) *Active interposer*: Active interposers are manufactured to include active transistor devices within the interposer, providing several unique capabilities not possible with passive interposers. We model these interposers as an additional large die that is typically in an older technology node when compared to the chiplets and are patterned with both FEOL layers for active silicon and BEOL layers for interconnects. However, unlike a regular chiplet, the active region is only restricted to local regions with routers and repeaters.

We use a similar model based on Equation (4) to estimate CFP overhead from active interposer. Interposer-based packaging architectures have higher CFP when compared to the RDL fan-out-based packaging and EMIB-based packaging as the interposer acts as an additional large silicon die that spans the entire area of all the chiplets put together with BEOL layers across the entire interposer and active FEOL layers locally in those areas that have routers or repeaters.

(d) *Passive interposer*: Unlike active interposers, passive interposers only contain metal interconnect, so they cannot include active logic like routers, or repeaters in the interposer. We model the CFP of the passive interposer in a similar way as Equation (5) on a per unit area and per layer basis.

It is important to note here that the overheads from the package substrate are the same across all architectures and is also going to be a part of the monolithic system. Therefore, we do not account for the CFP due to package substrates. The package substrate of a HI system is larger than that

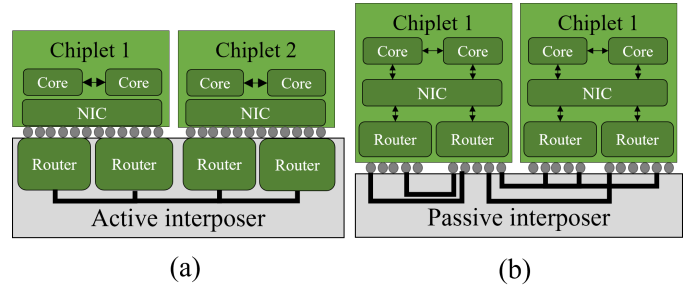


Fig. 4. Router location in the (a) active and (b) passive interposer.

of a monolithic system, and the additional CFP due to the area overheads are considered after estimating the area of the package using our whitespace estimator algorithm.

(2) *Inter-die communication overheads* ($C_{\text{mfg, comm}}$): Unlike EMIB and RDL-based packaging architectures, which are limited to supporting few (four - five) chiplets [24], interposer-based packaging architectures support tens of chiplets, but come at large inter-die communication overheads which are protocols such as network on-chip (NoC). To support an NoC router, each chiplet must be equipped with a network interface controller (NIC) as shown in Fig. 4. In passive interposers, router modules must be placed on the chiplets, as shown in Fig. 4(b), contributing to chiplet area and degrading yield and $C_{\text{mfg, i}}$ while with active interposers, router modules can be moved from the chiplets to the interposer, reducing the area in the chiplets, as shown in Fig. 4(a) and therefore improving chiplet yield and $C_{\text{mfg, i}}$ compared to passive interposers.

To estimate the CFP overheads of routing, we model the area overhead for NoC routers which in turn depends on the technology node in which the router is implemented, the number of ports, and the flit widths [38], [39]. The CFP overhead for interposer-based NoC routers for inter-die communication is given by: $C_{\text{mfg, comm}} = \text{CFPA} \times A_{\text{router}}(d, p)$, where CFPA is defined in (4). For the passive interposer, $A_{\text{router}}(d, p)$ is added to the area of the chiplet, after which yield and $C_{\text{mfg, i}}$ is calculated. For active interposers, the carbon contribution of $A_{\text{router}}(d, p)$ is used to add to the overall CFP of the system directly. It’s important to note that for passive interposers, the NoC is implemented in the same technology node as the chiplet, which is a more advanced node than those routers that are a part of the package. Therefore, routers for passive interposers are of lower areas than the active interposer router in an older technology node. For EMIB- and RDL-based packages there are additional communication overheads for PHY [37] interfaces that are typically part of the chiplet itself. These interfaces are typically designed as IPs and have small additional areas when compared to the chiplets.

(3) *Whitespace overheads* ($C_{\text{whitespace}}$): We develop a whitespace estimation algorithm that performs recursive bi-partitioning to build a slicing floorplan of the chiplets on the package substrate/interposer. An initial two-way partition is created by assigning the chiplets (sorted in decreasing order of their area), one by one, to the partition with a lesser total weight. Our model uses the area of each partition as the weight, which results in an area-balanced initial partition. The bi-partitioning procedure is then used recursively within

each partition to perform a K-way partition of the chiplets by first creating two equal-sized partitions, then independently dividing each of these into two subpartitions each, and so on till a partition contains only one chiplet. This effectively creates a full binary tree where each leaf node is a chiplet and each internal node represents a partition. The overall floorplan and its area can be derived by processing the partitions and chiplets within the tree.

For each leaf node, processing involves setting the orientation and aspect ratio of the chiplet to get a bounding box. At the internal nodes, this involved combining two subpartitions together, accounting for whitespace overheads. There are two sources of whitespace overheads: (i) some spacing between two subpartitions due to chiplet spacing constraints [38], [40], (ii) if the two subpartitions are imbalanced in terms of their dimensions, we created a bounding box of the two partitions which will result in whitespace. The recursive bipartisan floorplan also provides us with interfaces between each pair of chiplets to identify locations for routers, and silicon bridges on the package substrate/interposer.

D. Design CFP estimation

Although design CFP (C_{des}) is amortized across the number of chips manufactured, several cutting-edge accelerators, GPUs, and server CPUs are not manufactured in sufficiently large numbers to amortize the cost of design across the number of parts manufactured. We model the design CFP, C_{des} as:

$$C_{des} = \frac{\sum_{i=1}^{N_C} C_{des,i} + C_{des,comm}}{N_P} \quad (7)$$

where $C_{des,i} = t_{des,i} \times P_{des} \times C_{des,src}$ is the design CFP of a single chiplet, $C_{des,comm}$ is the design CFP of routers for interdie communication, N_P is the number of parts manufactured, $t_{des,i}$ is the CPU compute time it takes to design a chip/chiplet, P_{des} is the power consumed by the compute resources (CPUs) used to design the chips, $C_{des,src}$ is the CFP of the energy source. We model $t_{des,i}$ as:

$$t_{des,i} = \frac{t_{verif,i} + (t_{SP\&R,i} + t_{analyze,i}) \times N_{des}}{\eta_{EDA}} \quad (8)$$

where $t_{verif,i}$, $t_{SP\&R,i}$, $t_{analyze,i}$ are the compute time for verification, and a single synthesis, place, and route (SP&R) run and a single simulation of all analysis respectively, and N_{des} is the number of design iterations. Further, with EDA tools improving with every new version release due to advances made by EDA research groups. We create a near-linear regression model to predict EDA tool improvements with every new version released based on the data from [27] and scale the value of $t_{des,i}$ by η_{EDA} to model EDA tool productivity.

IV. EVALUATION OF CFP ANALYSIS TOOL

A. Methodology and experimental setup

(1) *Input parameters* Our CFP estimator, developed in Python3.7, uses several input parameters which are listed in Table I with their supported range of values and their sources. For instance, based on the source of energy, whether it is coal, gas, wind etc, the $C_{mfg,src}$ can be a value between 30g – 700g

TABLE I
LIST OF INPUT PARAMETERS TO OUR EMBODIED CFP ESTIMATION TOOL AND THEIR RANGE OF VALUES AND SOURCES.

Model	Parameter	Value	Unit	Source
$C_{mfg,i}$	$D0(p)$	0.07 – 0.3	/cm ²	[31], [32]
	α	3		[31], [32]
	$D_T(d, p)$	5 – 150	MTr/mm ²	[28], [29]
	$\eta_{eq}(p)$	0 – 1		[13]
	$C_{mfg,src}$	30 – 700	g CO ₂ /kWh	[4], [5]
	$EPA(p)$	0.8 – 3.5	kWh/cm ²	[4], [5]
	C_{gas}	0.1 – 0.5	kg CO ₂ /cm ²	[4], [5]
$C_{package}$	$C_{material}$	0.5	kg CO ₂ /cm ²	[4], [5]
	RDL tech.	22nm – 65nm		[24], [37], [38]
	$EPLA_{RDL}(p)$	0.05 – 0.2	kWh/cm ²	[4], [5]
	$C_{pkg,src}$	30 – 700	g CO ₂ /kWh	[4], [5]
	L_{RDL}	3 – 4		[24]
	L_{bridge}	3 – 4		[37]
	Bridge tech.	22nm – 65nm		[37]
$C_{mfg,comm}$	$EPLA_{bridge}(p)$	0.1 – 0.35	kWh/cm ²	[4], [5]
	Bridge range	2 × 2	mm ²	[37]
	Interposer tech.	22nm – 65nm		[38]
$C_{whitespace}$	NoC flit width.	512 bits		[38]
	Chiplet spacing	0.1 – 1	mm	[38], [40]
C_{des}	η_{EDA}	0 – 1		[27]
	P_{des}	10	W	[41]
	N_{des}	100		[42]
	$C_{des,src}$	30 – 700	g CO ₂ /kWh	[4], [5]

of CO₂ or based on the technology node, the defect densities can be between 0.07 – 0.3/cm² [24].

Although our simulator can handle a range of technology nodes for packaging and a range of derate factors for $C_{mfg,src}$, as highlighted in the table, our results in this section are shown for specific values, i.e., we assume all packaging technology (RDL, EMIB, and active/passive interposers) to be in 65nm and the energy source is from coal at 700g of CO₂ per kWh. Based on the testcase, we vary the technology node for each of the chiplets to explore the possible design space and estimate $C_{mfg,i}$. Based on the technology each chiplet is implemented in, we choose the appropriate values from the specified ranges. (2) *Testcases and architectures* We evaluate our carbon simulator on four industry testcases: (i) Intel mobile processor, Tiger Lake(2020) [43], (ii) Intel server-class 2-chiplet-based CPU, Emerald Rapids (EMR) [44] (to be released in Q4 2023), (iii) NVIDIA GA102 GPU (2020) [45], and (iv) Apple A15 SoC (2021) [46]. The input to our simulator is an architectural description of these testcases with the die area breakdowns for each of these processors. We obtain the area breakdowns of each of these testcases from third-party websites such as [43]–[45], [47]. For the monolithic SoCs (Tiger Lake, GA102, and A15) we break them into chiplets based on the block-level architecture. We use one chiplet for memory, another chiplet for analog components, and a third chiplet for digital logic inspired by [15]. We also further explore the design space by splitting the large digital logic chiplet into smaller chiplets. For Intel Emerald Rapids, an EMIB-based 2-chiplet testcase, we perform CFP estimation for the original chiplet-based architecture. We also perform carbon evaluation on a 4-chiplet version of the same testcase where we split the large digital logic blocks into two smaller chiplets each.

In the rest of this section, we use the NVIDIA GA102 testcase as a case study and show detailed results on each of the components (manufacturing, packaging, and design) of the total embodied CFP for different possible chiplet architectures

and compare it to the CFP of the monolithic SoC. Next, in the interest of space, for the rest of the three testcases, we only summarize the manufacturing and packaging CFP and compare that to its monolithic counterpart.

B. Example case study: NVIDIA GPU GA102

As an example case study, we use the NVIDIA GPU GA102 architecture to evaluate the various components of embodied CFP for various chiplet disaggregation scenarios of the test-case. The first set of results is for three-chiplet scenario where one of the chiplets implements memory, the other analog components, and the third digital blocks. The next set of results will show the CFP for a general N_c -chiplet architecture.

(1) *Manufacturing and packaging CFP for three chiplets* The manufacturing CFP of GA102, for different configurations of technology nodes for each chiplet, is shown in Fig. 5(a). The x-axis lists the technology nodes where the lowermost row is the technology node for the digital logic, the middle row is analog components (IOs), and the topmost row is memory. The (7,7,7) scenario is a monolithic representation of the architecture of a single die in a 7nm node. It, therefore, does not have the additional HI-related packaging overheads, but includes packaging overheads as a part of manufacturing carbon using models from [4]. The figure shows that the lowest embodied CFP is for the (7, 14, 10) scenario. This is because the analog components and memory blocks [15] do not scale in the area as much as the digital blocks and can therefore be implemented in an older technology node with almost the same area. On the contrary, in the (10, 10, 10) scenario, the digital logic scales to a much larger area and therefore has a larger CFP than even the monolith resulting in a larger CFP even though the 10nm node has a lower defect density and lower CFP when compared to 7nm. The packaging overhead values in this figure are for an RDL-based package with the RDL layers implemented in a 65nm technology node. The packaging overhead has also accounted for the whitespace between the three chiplets and routing overheads. From this result, it is clear that HI enables using chiplets that have small areas and higher yields, which helps lower the CFP, and the further integration of chiplets in different technology nodes can further lower the CFP as older nodes have lower EPA than advanced nodes.

(2) *Design CFP for three chiplets* From our experiments in performing SP&R of large designs, we find that the $t_{SP\&R,i}$ for a design with 700,000 logic gates in a 7nm commercial technology is about 24 CPU hours. These estimates are on a 192GB RAM machine with a dual-core Intel Xeon CPU with 8 threads, each running at a 2.4GHz clock frequency. Therefore, extending this model to the NVIDIA GA102 testcase, $t_{SP\&R,i} = 1.2 \times 10^6$ CPU hours as it has over 4.5B logic gates. Assuming $P_{des} = 10W$ [41] and the energy supplied comes from non-renewable sources, then a single run of SP&R results in 8,400kg of CO₂ equivalent emission in the 7nm technology node. Fig. 5(b), shows the design carbon for a **single iteration** of SP&R for the three chiplet testcase. Older technology nodes have lower design times due to EDA tool scaling [27], and therefore, have lower CFP when compared to the monolithic

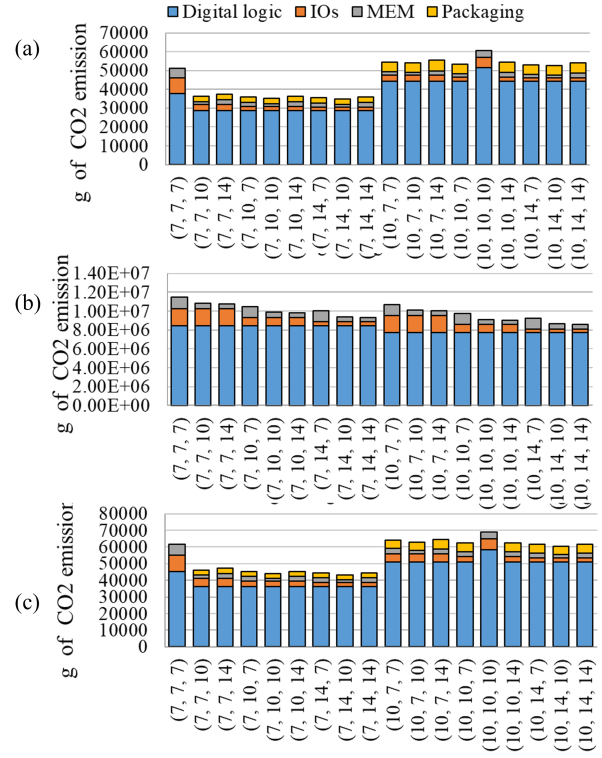


Fig. 5. (a) Manufacturing and packaging CFP, (b) design CFP for a **single iteration** of SP&R, and (c) overall CFP for different configurations of three chiplets for the NVIDIA GA102 architecture with RDL fan-out package.

SoC in an advanced 7nm technology. In addition, since HI enables the “reuse” of pre-designed chiplets, in principle, the entire digital logic chiplet can be reused for another design saving the entire associated design CFP.

Although, the CFP values in Fig. 5(b) are significantly large, these costs are amortized across the number of parts manufactured (N_p). The figure only shows the results for a single iteration of SP&R. However, with hundreds ($N_{des} = 100$) of design iterations and SP&R runs and verification dominating 80% of the product development time, the design of an IC can easily contribute to over 2,000,000kg of CO₂ equivalent emission, assuming all compute energy is coming from non-renewable sources. Assuming the number of manufactured parts is $N_p = 200,000$, the SP&R carbon cost gets amortized to 12kg of CO₂ equivalent emission per IC, which is more than 25% of the manufacturing carbon cost (see Fig. 5(a)).

(3) *Total embodied CFP for three-chiplet architecture* To estimate the total embodied CFP, we sum the manufacturing and packaging costs from Fig. 5(a) and amortized design costs assuming, $N_p = 200,000$ and $N_{des} = 100$ from Fig. 5(b). Fig. 5(c) shows the total embodied CFP of all three components for different configurations of the three chiplet-based GA102 testcase. The (7, 14, 10) configuration has the least CFP showing the potential of HI to bringing down CFP.

(4) *Total embodied CFP with N_c chiplets* In addition to the three chiplet architecture of GA102, we also evaluate the manufacturing and packaging carbon for $N_c > 3$ where we take the digital logic in 7nm and further split the logic block into smaller chiplets each implemented in 7nm. The analog

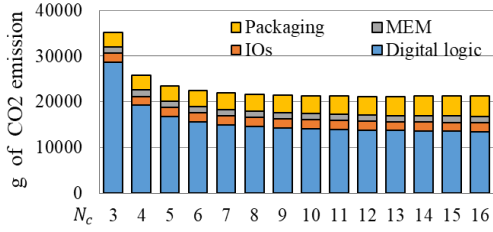


Fig. 6. C_{mfg} and C_{HI} for N_c chiplets on the NVIDIA GA102 GPU testcase.

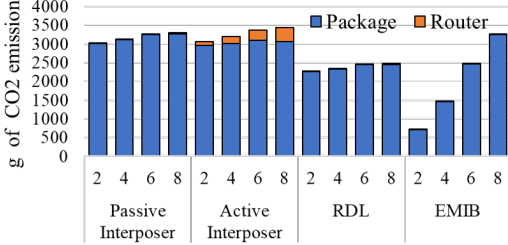


Fig. 7. Packaging CFP overheads for different N_c values.

(IOs) and memory chiplets are in 14nm and 10nm, respectively. Fig. 6 shows the manufacturing and packaging CFP for different N_c . As N_c increases, the chiplet manufacturing CFP decreases due to smaller chiplets and better yields, while the packaging CFP increases due to larger HI overheads.

(5) *Packaging CFP for different architectures* To understand the differences in CFP overheads of the four different packaging architectures considered, we use the large digital logic component of GA102 as an example testcase. We split the 500mm² monolithic digital logic block into N_c different chiplets and evaluate C_{HI} . Fig. 7 shows the difference in CFP for these architectures separated by routing overheads and package-related overheads (whitespace and area). For the four architectures, all the interconnects in the package substrate are modeled in a 65nm technology.

Silicon-bridge-based (EMIB-based) architectures have the least CFP for 2- and 4-chiplet-based architectures of the 500mm² monolith testcase. However, as N_c increases, the number of silicon bridges also increases, and CFP increases. The RDL-based packages have the least overheads for the 6- and 8-chiplet architectures, but due to their architecture definition, they have lower communication bandwidth when compared to silicon bridges or interposers. Therefore, based on the bandwidth requirements of the testcase, such tradeoffs between performance and CFP can be considered using our analysis tool. The figure also shows that the passive interposer has lower routing overheads as the router is part of the chiplet and is in the same technology node of the chiplet. Therefore, in passive interposer technologies, due to the advanced node (7nm in this testcase) in which the router is implemented, the area overheads are smaller when compared to the 65nm router in the active interposer. The routing overheads of RDL, passive interposer, and silicon-bridge (EMIB) architectures are small and near-negligible when compared to the core chiplet areas.

C. Summary for different testcases

In Table II, we compare the embodied (design, HI, and manufacturing) CFP of a HI-based architecture against their

TABLE II
EMBODIED CFP (GRAMS OF CO₂ EMISSION) FOR CHIPLLET-BASED AND MONOLITHIC VERSIONS OF INDUSTRY TESTCASES.

Carbon	EMR 2-chiplet	EMR 4-chiplet	GA102	Apple A15	Tiger Lake
$C_{\text{mfg,chiplet1}}$	5.49E+04	2.06E+04	1.92E+03	1.28E+02	4.81E+02
$C_{\text{mfg,chiplet2}}$	5.49E+04	2.06E+04	1.40E+03	4.17E+02	2.44E+02
$C_{\text{mfg,chiplet3}}$	–	2.06E+04	9.62E+03	1.53E+03	4.95E+02
$C_{\text{mfg,chiplet4}}$	–	2.06E+04	9.62E+03	1.53E+03	–
$C_{\text{HI, RDL}}$	7.49E+03	9.95E+03	2.78E+03	5.99E+02	2.40E+02
$C_{\text{HI, EMIB}}$	9.63E+02	2.22E+03	1.47E+03	7.30E+02	4.87E+02
$C_{\text{HI, passive}}$	9.98E+03	1.33E+04	3.70E+03	7.93E+02	3.15E+02
$C_{\text{HI, active}}$	1.00E+04	1.34E+04	3.76E+03	8.41E+02	3.49E+02
C_{des}	1.19E+04	1.39E+04	4.70E+03	1.13E+03	2.63E+02
CFP_{tot} (RDL)	1.29E+05	1.06E+05	3.00E+04	5.34E+03	1.72E+03
CFP_{tot} (EMIB)	1.23E+05	9.85E+04	2.87E+04	5.47E+03	1.97E+03
CFP_{tot} (passive)	1.32E+05	1.10E+05	3.10E+04	5.53E+03	1.80E+03
CFP_{tot} (active)	1.32E+05	1.10E+05	3.10E+04	5.58E+03	1.83E+03
Monolithic	2.55E+05	2.91E+05	5.58E+04	5.60E+03	1.96E+03

monolithic SoC counterparts for different testcases, different packaging architectures, and a specific configuration of chiplets. The EMR 2-chiplet represents the architecture of the Intel Emerald Rapids (EMR) testcase, where both chiplets are in 7nm technology nodes. We create an EMR 4-chiplet testcase where we further split the two chiplets in EMR into four based on the Intel Sapphire Rapids architecture [48], all implemented in a 7nm technology. The table also lists 4-chiplet versions of NVIDIA GPU GA102, and Apple A15 SoC, where the memory is implemented in 10nm, IOs/analog chiplets are implemented in 14nm, and the two digital logic chiplets in 7nm. The Tiger Lake testcase split into three chiplets for memory (10nm), analog (14nm), and digital logic (7nm).

For the above-described testcases, the table lists $C_{\text{mfg},i}$ for each chiplet, C_{HI} for different packaging architectures, the C_{des} assuming $N_{\text{des}} = 100$ and $N_p = 200,000$, and the total CFP for each testcase compared against its monolithic counterpart. We find that the total CFP of the HI-based testcases are all lower than their monolithic counterparts. For instance, the EMR 2-chiplet and 4-chiplet testcases with silicon bridge-based packages have 55% and 70% lower CFP when compared to their monolithic counterparts. We also observe that HI systems have a higher benefit with embodied CFP for large SoC testcases when compared to the smaller ones. For example, the GA102, and EMR testcases have large monolithic areas of approximately 500mm² and 1500mm², respectively, while the Apple A15 and Tiger Lake testcases have areas of over 100mm², and therefore the larger testcases, have a significantly higher improvement in CFP.

V. CONCLUSION

In this paper, we proposed HI as a path towards sustainable computing by designing and manufacturing chiplet-based systems with lower embodied carbon footprint (CFP) than monolithic SoCs. We have developed an embodied CFP estimator that uses architectural-level descriptions to assess CFP of heterogeneous systems. The simulator can be used to guide optimization during system disaggregation. If this paper is accepted, we will open-source the CFP simulator for broader community use.

REFERENCES

- [1] C. Freitag, *et al.*, “The real climate and transformative impact of ICT: A critique of estimates, trends, and regulations,” *Patterns*, vol. 2, no. 9, p. 100340, 2021.
- [2] B. Graver, *et al.*, “CO2 emissions from commercial aviation,” 2019. <https://theicct.org/publication/co2-emissions-from-commercial-aviation-2018/> (last accessed: March 2023).
- [3] L. Å. Ragnarsson, *et al.*, “The green transition of the IC industry,” 2022. <https://www.imec-int.com/en/expertise/cmos-advanced/sustainable-semiconductor-technologies-and-systems-sstss/stss-white-paper> (last accessed: March 2023).
- [4] U. Gupta, *et al.*, “ACT: Designing sustainable computer systems with an architectural carbon modeling tool,” in *Proceedings of the ACM International Symposium on Computer Architecture*, p. 784–799, 2022.
- [5] M. Garcia Bardon, *et al.*, “DTCO including sustainability: Power-performance-area-cost-environmental score (PPACE) analysis for logic technologies,” in *Proceedings of the IEEE International Electron Devices Meeting*, pp. 41.4.1–41.4.4, 2020.
- [6] Apple, “Environmental responsibility report,” 2019. https://www.apple.com/environment/pdf/Apple_Environmental_Responsibility_Report_2019.pdf.
- [7] Facebook, “Facebook sustainability data 2019,” 2019. https://sustainability.fb.com/wp-content/uploads/2020/05/2019-Sustainability-Data-Disclosure_Final-1.pdf.
- [8] Microsoft, “Environmental sustainability report,” 2021. <https://www.microsoft.com/en-us/corporate-responsibility/sustainability/report>.
- [9] L. Eeckhout, “A first-order model to assess computer architecture sustainability,” *IEEE Computer Architecture Letters*, vol. 21, no. 2, pp. 137–140, 2022.
- [10] L. Eeckhout, “Kaya for computer architects: Toward sustainable computer systems,” *IEEE Micro*, vol. 43, no. 1, pp. 9–18, 2023.
- [11] U. Gupta, *et al.*, “Chasing carbon: The elusive environmental footprint of computing,” *IEEE Micro*, vol. 42, p. 37–47, jul 2022.
- [12] “Kaya identity.” https://en.wikipedia.org/wiki/Kaya_identity.
- [13] TSMC, “Corporate social responsibility report,” 2018. https://esg.tsmc.com/download/file/2018_tsmc_csr_report_published_May_2019/english/pdf/e_all.pdf.
- [14] C.-H. Kuo, *et al.*, “Life cycle impact assessment of semiconductor packaging technologies with emphasis on ball grid array,” *Journal of Cleaner Production*, vol. 276, p. 124301, 12 2020.
- [15] S. Naffziger, *et al.*, “AMD chiplet architecture for high-performance server and desktop products,” in *Proceedings of the IEEE International Solid-State Circuits Conference*, pp. 44–45, 2020.
- [16] M. T. Bohr and I. A. Young, “CMOS scaling trends and beyond,” *IEEE Micro*, vol. 37, no. 6, pp. 20–29, 2017.
- [17] S. S. Iyer, “Heterogeneous integration for performance and scaling,” *IEEE Transactions on Components, Packaging and Manufacturing Technology*, vol. 6, no. 7, pp. 973–982, 2016.
- [18] P. Gelsinger, “Keynote: Semiconductors run the world.” HotChips, 2022.
- [19] R. Mahajan, *et al.*, “Embedded multi-die interconnect bridge (EMIB) – a high density, high bandwidth packaging interconnect,” in *Proceedings of the IEEE Electronic Components and Technology Conference*, pp. 557–565, 2016.
- [20] S. Y. Hou, *et al.*, “Wafer-level integration of an advanced logic-memory system through the second-generation CoWoS technology,” *IEEE Transactions on Electron Devices*, vol. 64, no. 10, pp. 4071–4077, 2017.
- [21] D. B. Ingerly, *et al.*, “Foveros: 3D integration and the use of face-to-face chip stacking for logic devices,” in *Proceedings of the IEEE International Electronic Devices Meeting*, pp. 19.6.1–19.6.4, 2019.
- [22] Y. H. Chen, *et al.*, “Ultra high density SoIC with sub-micron bond pitch,” in *Proceedings of the IEEE Electronic Components and Technology Conference*, pp. 576–581, 2020.
- [23] IEEE Components and Packaging Society, “Heterogeneous integration roadmap,” 2021. <http://eps.ieee.org/hir>.
- [24] J. H. Lau, “Recent advances and trends in advanced packaging,” *IEEE Transactions on Components and Packaging Technologies*, vol. 12, no. 2, pp. 228–252, 2022.
- [25] D. B. Ingerly, *et al.*, “Foveros: 3d integration and the use of face-to-face chip stacking for logic devices,” in *Proceedings of the IEEE International Electronic Devices Meeting*, pp. 19.6.1–19.6.4, 2019.
- [26] W. Gomes, *et al.*, “Meteor Lake and Arrow Lake Intel next-gen 3D client architecture platform with Foveros,” in *Proceedings of the IEEE Hot Chips Symposium*, pp. 1–40, Aug. 2022.
- [27] J. Ferguson, “EDA innovation is the foundation of progress.” <https://www.techdesignforums.com/practice/technique/physical-verification-eda-innovation-is-the-foundation-of-progress/>.
- [28] Angstromics, “The Truth of TSMC 5nm.” <https://www.angstromics.com/p/the-truth-of-tsmc-5nm>.
- [29] D. Schor, “IEDM 2022: Did we just witness the death of SRAM?,” <https://fuse.wikichip.org/news/7343/iedm-2022-did-we-just-witness-the-death-of-sram/>.
- [30] J. Cunningham, “The use and evaluation of yield models in integrated circuit manufacturing,” *IEEE Transactions on Semiconductor Manufacturing*, vol. 3, no. 2, pp. 60–71, 1990.
- [31] A. Ning, *et al.*, “Supply chain aware computer architecture,” in *Proceedings of the ACM International Symposium on Computer Architecture*, 2023. <https://augustning.com/assets/papers/supply-chain-isca-2023-preprint.pdf>.
- [32] D. Stow, *et al.*, “Cost-effective design of scalable high-performance systems using active and passive interposers,” in *Proceedings of the IEEE/ACM International Conference on Computer-Aided Design*, pp. 728–735, 2017.
- [33] T. Li, *et al.*, “Chiplet heterogeneous integration technology—status and challenges,” *Electronics*, vol. 9, no. 4, 2020.
- [34] SPIL, “Corporate social responsibility report,” 2018. <https://www.spil.com.tw/Files/pdf-en/2018-en.pdf>.
- [35] Amkor Technology Inc., “Sustainability accounting standards board report,” 2021. <https://amkor.com/esg/esg-report/>.
- [36] ACE Group, “Corporate sustainability report,” 2017. <https://ase.aseglobal.com/en/csr/downloads/report>.
- [37] R. Mahajan, *et al.*, “Embedded multidie interconnect bridge—a localized, high-density multichip packaging interconnect,” *IEEE Transactions on Components, Packaging and Manufacturing Technology*, vol. 9, no. 10, pp. 1952–1962, 2019.
- [38] D. Stow, *et al.*, “Investigation of cost-optimal network-on-chip for passive and active interposer systems,” in *Proceedings of the ACM/IEEE International Workshop on System Level Interconnect Prediction (SLIP)*, pp. 1–8, 2019.
- [39] C. Sun, *et al.*, “Dsnt - a tool connecting emerging photonics with electronics for opto-electronic networks-on-chip modeling,” in *2012 IEEE/ACM Sixth International Symposium on Networks-on-Chip*, pp. 201–210, 2012.
- [40] S. Y. Hou, *et al.*, “Wafer-level integration of an advanced logic-memory system through the second-generation cowos technology,” *IEEE Transactions on Electron Devices*, vol. 64, no. 10, pp. 4071–4077, 2017.
- [41] “List of CPU power dissipation figures.” https://en.wikipedia.org/wiki/List_of_CPU_power_dissipation_figures.
- [42] P. Agrawal, *et al.*, “Optimal scheduling and allocation for ic design management and cost reduction,” *ACM Transactions on Design Automation of Electronic Systems*, vol. 22, jun 2017.
- [43] P. Alcorn, “Intel details Tiger Lake at Hot Chips 2020, die revealed.” <https://www.tomshardware.com/news/intel-details-tiger-lake-at-hot-chips-2020-die-revealed>.
- [44] D. Patel, *et al.*, “Intel Emerald Rapids backtracks on chiplets – design, performance & cost.” <https://www.semianalysis.com/p/intel-emerald-rapids-backtracks-on>.
- [45] Z. Liu, “IR photographer shares die shots of Nvidia 3000 series GA102 silicon.” <https://www.tomshardware.com/news/infrared-photographer-photos-nvidia-ga102-ampere-silicon>.
- [46] Wikipedia, “Apple a15 processor.” https://en.wikipedia.org/wiki/Apple_A15.
- [47] D. Patel, “Apple A15 die shot and annotation – IP block area analysis.” <https://www.semianalysis.com/p/apple-a15-die-shot-and-annotation>.
- [48] Wikipedia, “Sapphire rapids.” https://en.wikipedia.org/wiki/Sapphire_Rapids.